Supporting Information

Defect-mediated dual-site synergy in Zn-$CuInS_2$ enables orbital-tailored high performance photocatalytic CO_2-to-ethylene conversion

Kezhen Lai, [a] Yuxin Sun, [a] Linping Li, [a] Xiaoqing Shi, [a] Xiaosong Zhou,[c] Ning Li, [a] Yangqin Gao, [a, b] Lei Ge, [* a, b]

[a] State Key Laboratory of Heavy Oil Processing, College of New Energy and Materials, China University of Petroleum Beijing, No. 18 Fuxue Rd., Beijing 102249, People's Republic of China.

[b] Dongying Guoan Chemical Co., Ltd, Circular Economy Industrial Park, Lijin County, Dongying, Shandong Province, 257400, People's Republic of China.

[c] School of Chemistry and Chemical Engineering, Lingnan Normal University, Zhanjiang 524048, Guangdong, China

*Corresponding Author, E-mail: gelei08@sina.com, gelei@cup.edu.cn (Lei Ge).

1. Supplementary Figures

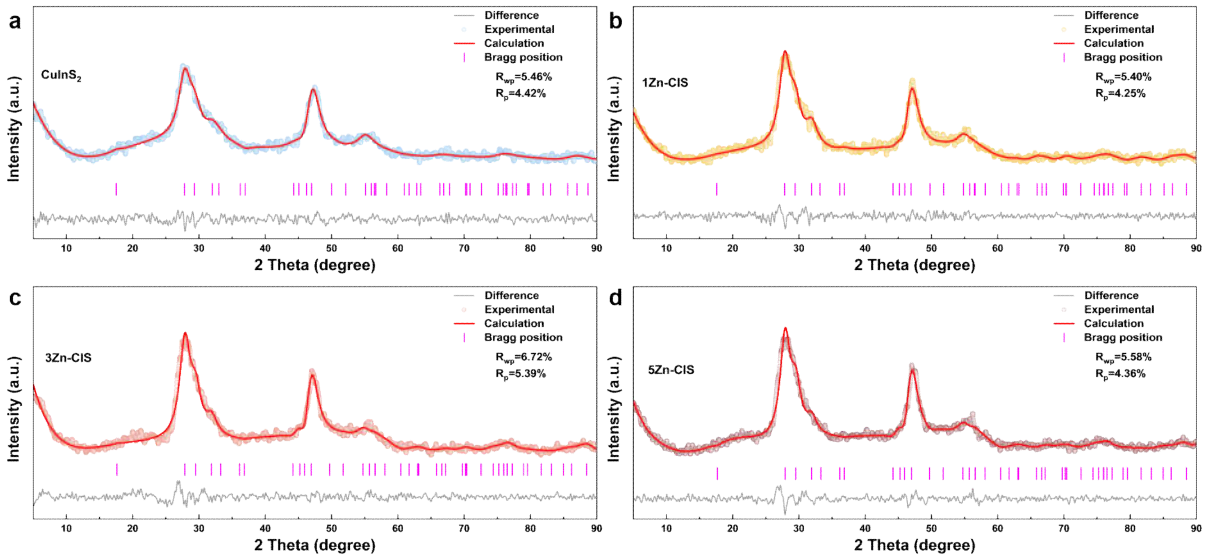

Fig. S1. The XRD data of (a) $CuInS_2$, (b) 1Zn-CIS, (c) 3Zn-CIS and (d) 5Zn-CIS fitted by Rietveld refinement.

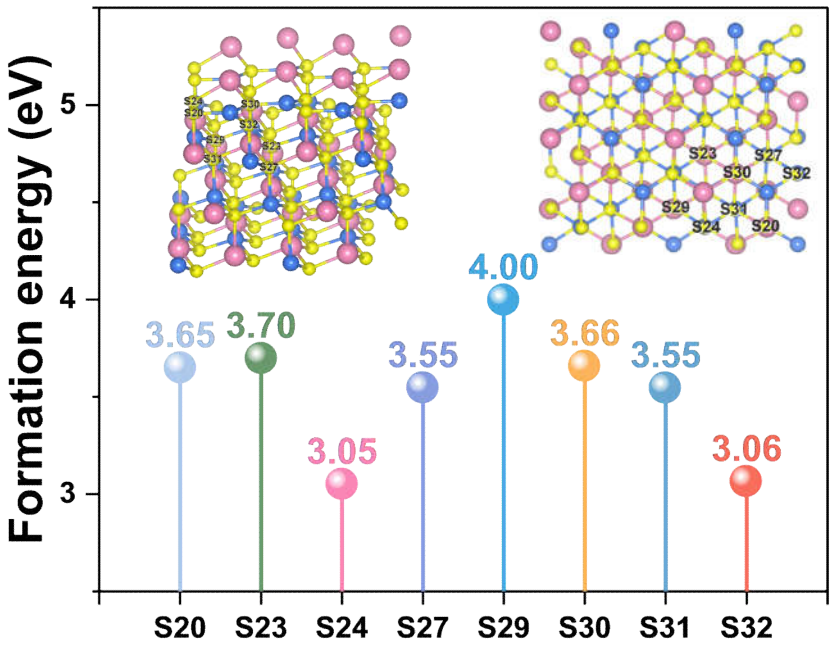

Fig. S2. The formation energy of S_v at different sites in the $CuInS_2$ model.

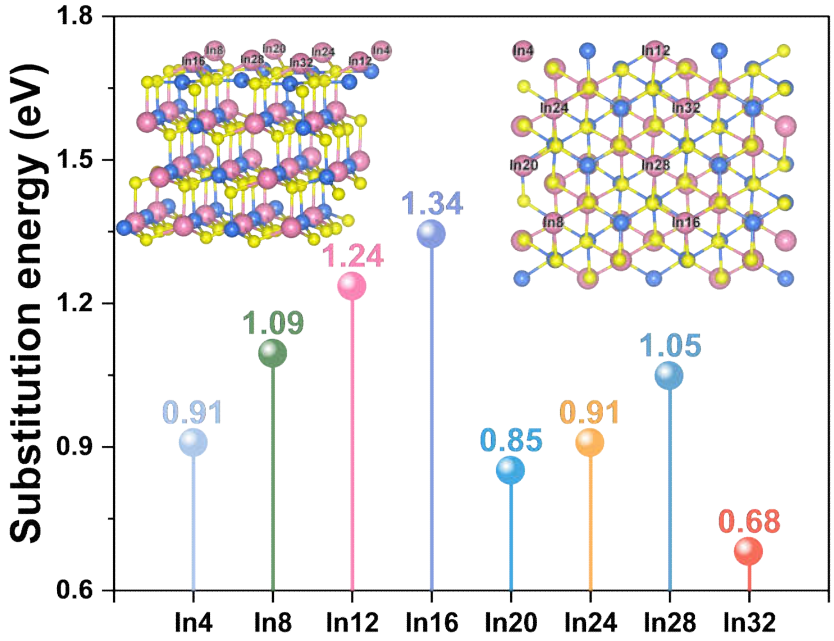

Fig. S3. The substitution energy of Zn replacing different In sites.

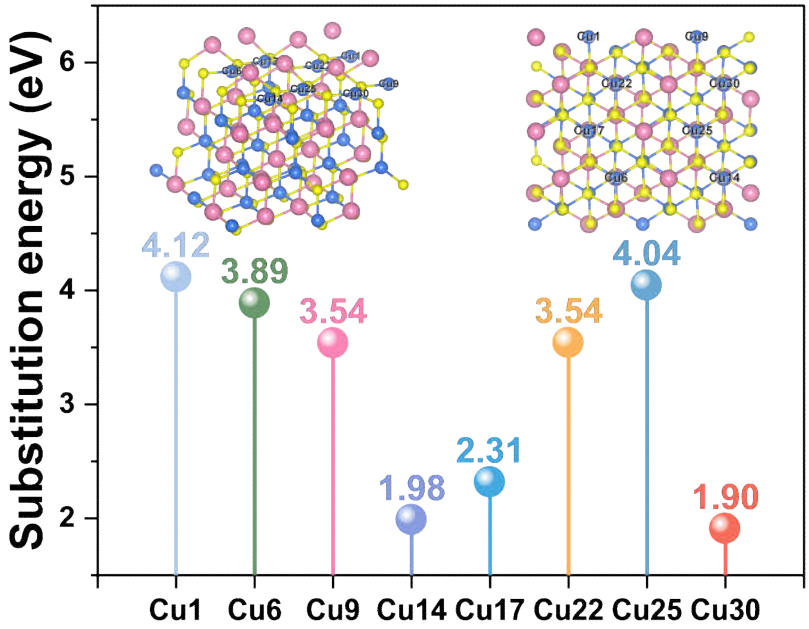

Fig. S4. The substitution energy of Zn replacing different Cu sites.

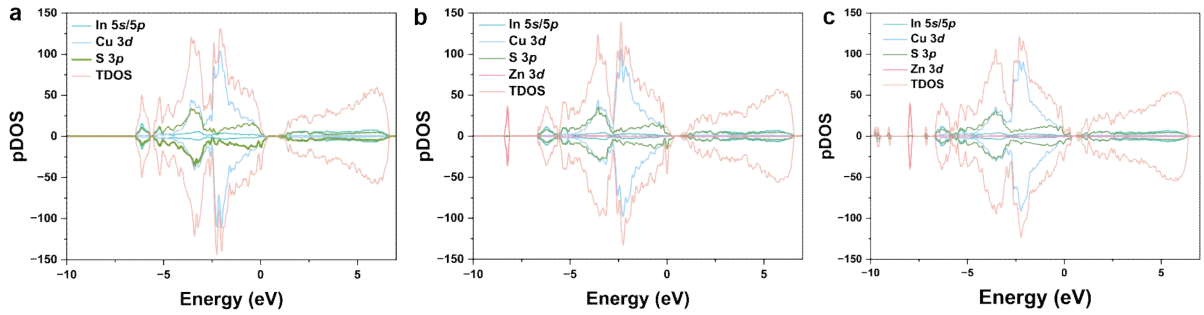

Fig. S5. The pDOS of (a) $CuInS_2$, (b) Zn-CIS without S_v and (c) Zn-CIS with S_v.

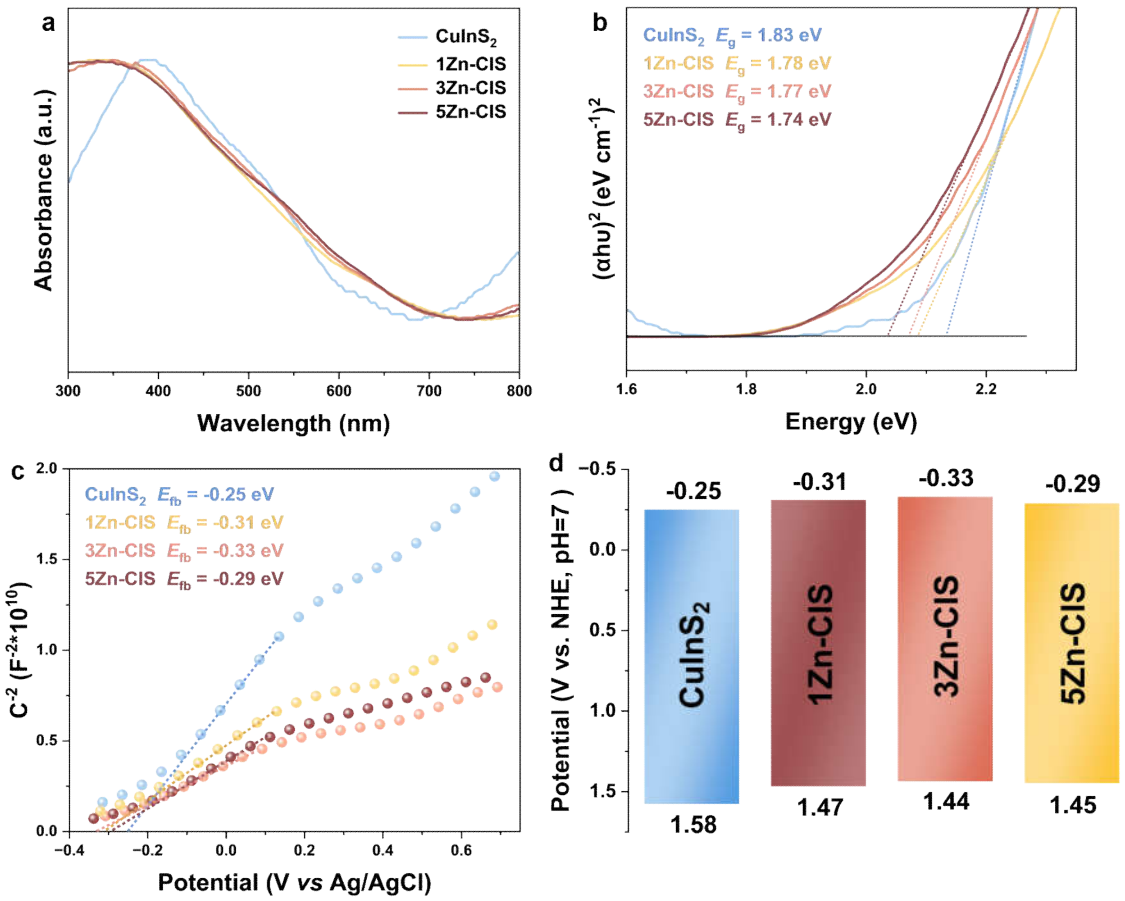

Fig. S6. (a) UV-vis DRS, (b) Tauc plot, (c) M-S plot and (d) band structure diagram of $CuInS_2$, 1Zn-CIS, 3Zn-CIS and 5Zn-CIS.

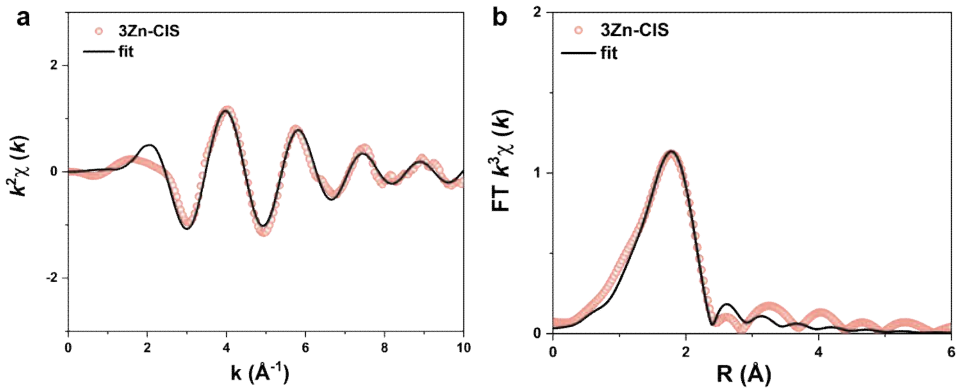

Fig. S7. (a) EXAFS fitting curve for 3Zn-CIS in the k-space, (b) EXAFS fitting curve for 3Zn-CIS in the R-space.

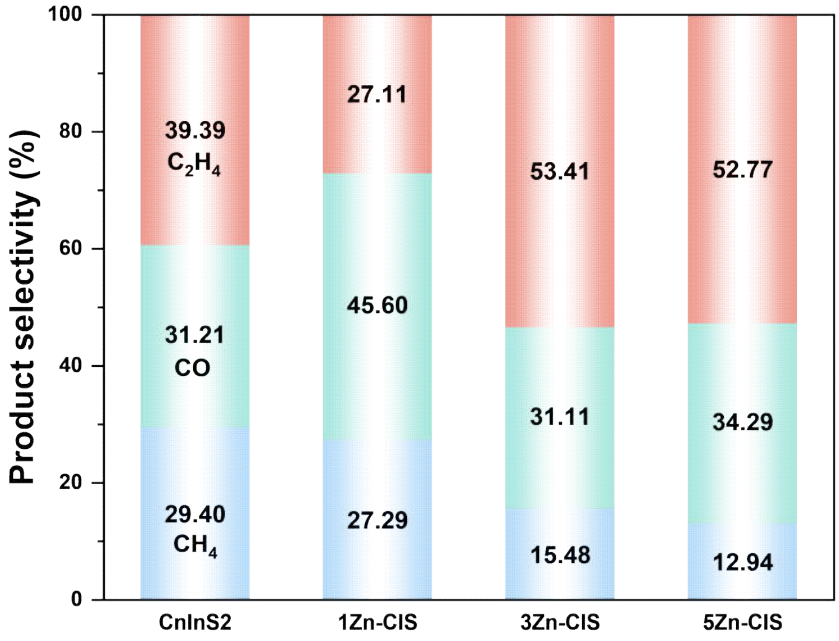

Fig. S8. The product selectivity of $CuInS_2$ and Zn-CIS.

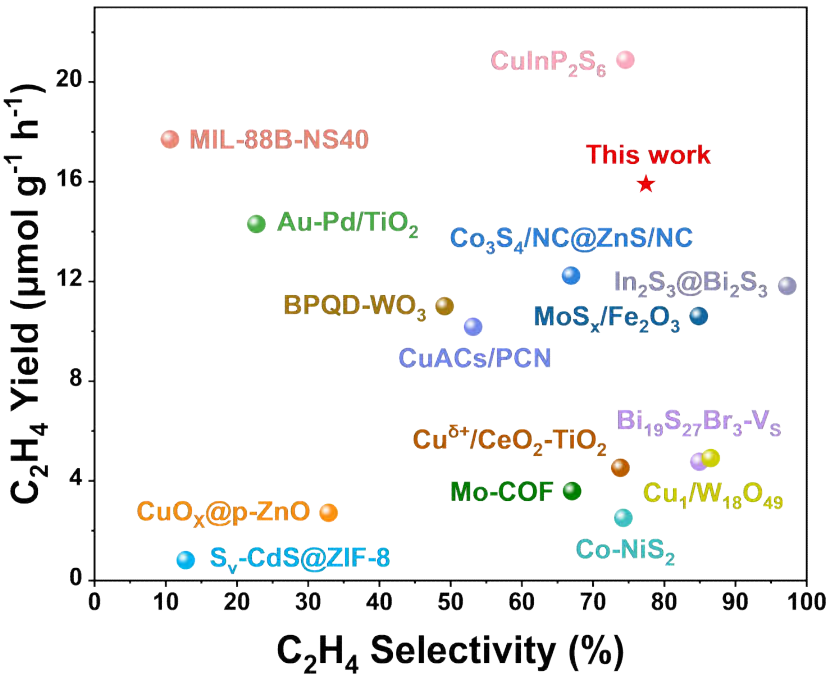

Fig. S9. The performance comparasion of C_2H_4 in our work with that in the previous literitures ($Cu^{\delta+}/CeO_2$-TiO_2 [1], CuACs/PCN [2], Au-Pd/TiO_2 [3], S_v-CdS@ZIF-8 [4], CuO_x@p-ZnO [5], Co-NiS_2 [6], Mo-COF [7], $CuInP_2S_6$ [8], MoS_x/Fe_2O_3 [9], $Cu_1/W_{18}O_{49}$ [10], α-Fe_2O_3/GR/Bi_2O_2S [11], V_S-$NiCo_2S_4$-NF [12], MIL-88B-NS40 [13], BPQD-WO_3 [14],$Bi_{19}S_{27}Br_3$-V_S [15], Co_3S_4/NC@ZnS/NC [16], In_2S_3@Bi_2S_3 [17]).

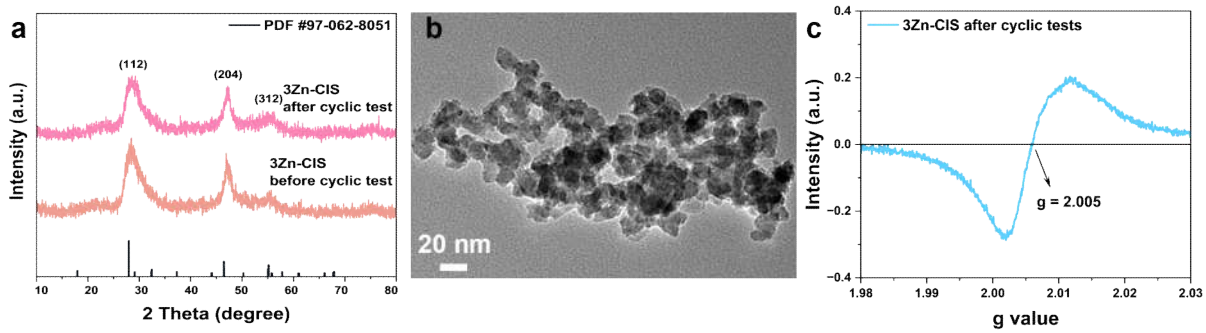

Fig. S10. (a) XRD pattern before and after cyclic stability test; (b) TEM image and (c) ESR after cyclic stability test.

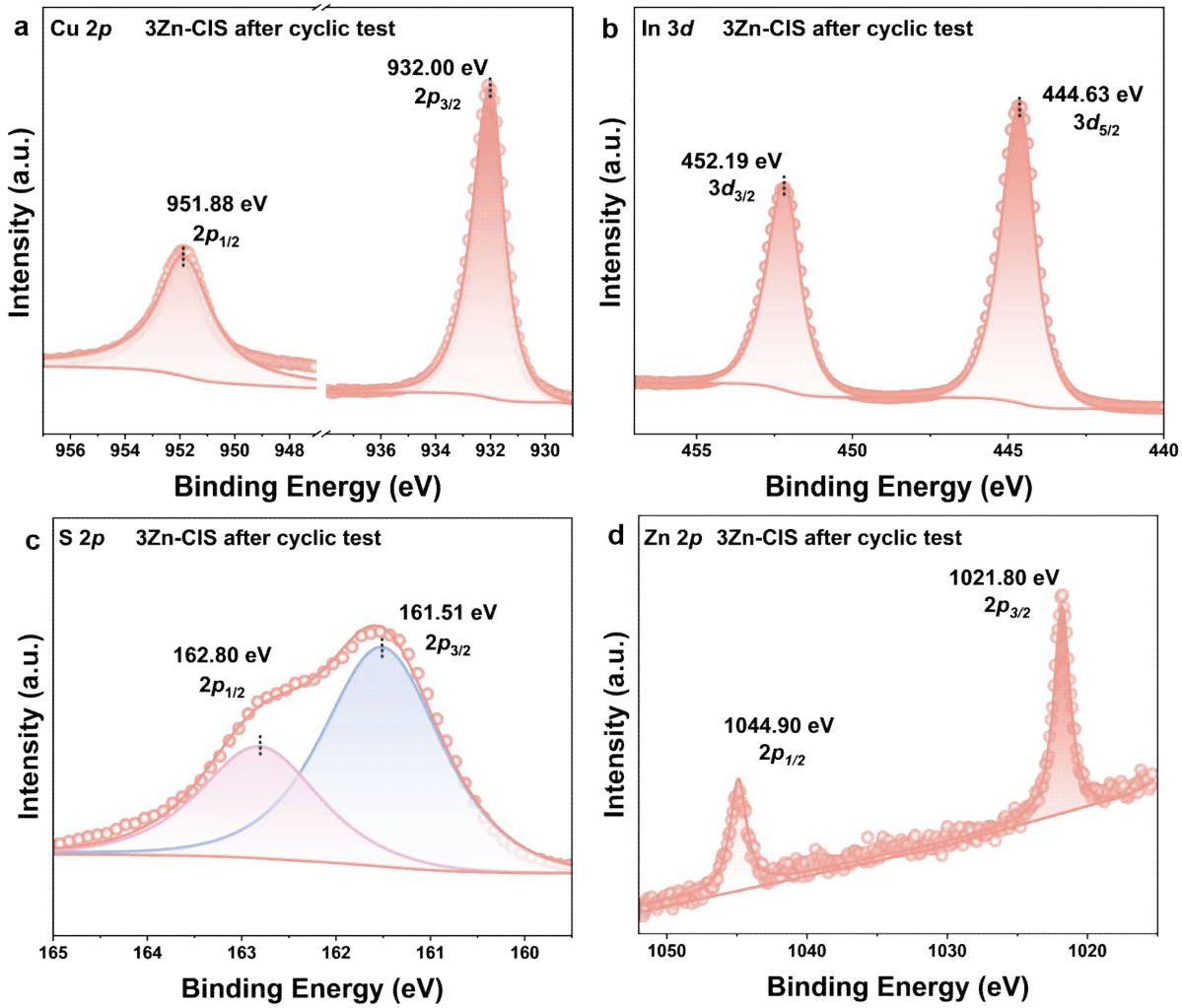

Fig. S11. The XPS spectra (a) Cu 2*p*, (b) In 3*d*, (c) S 2*p* and (d) Zn 2*p* after cyclic stability test.

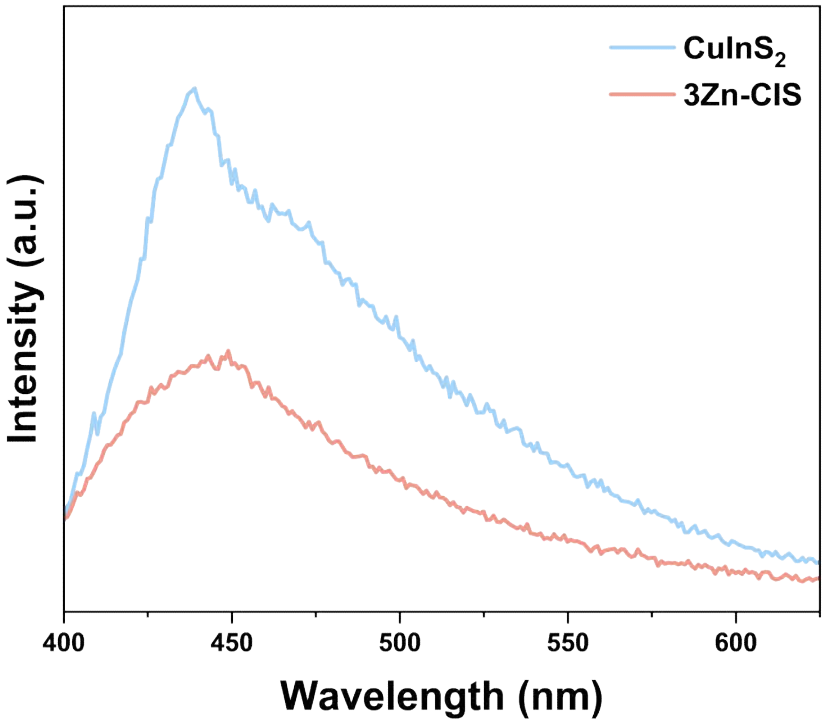

Fig. S12. PL spectrum of $CuInS_2$ and 3Zn-CIS.

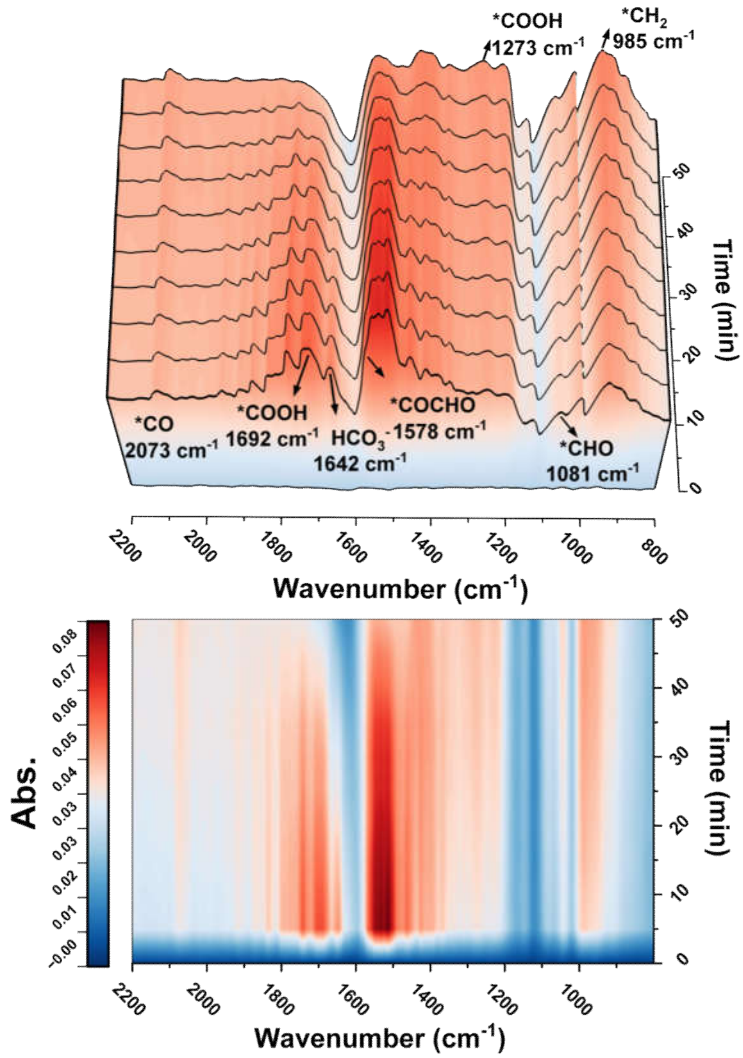

Fig. S13. *In situ* DRIFTS spectra of $CuInS_2$.

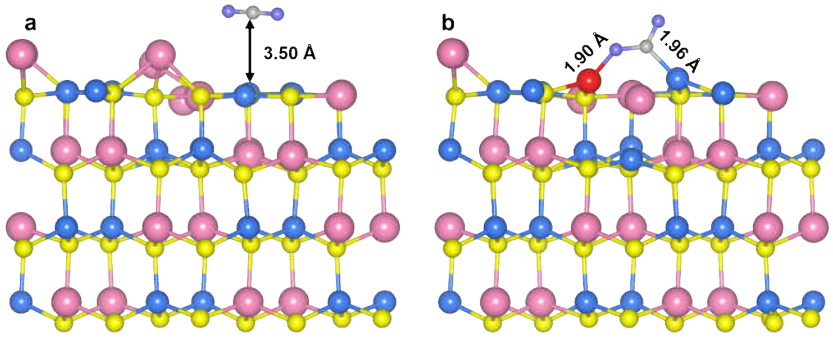

Fig. S14. The CO_2 adsorption model of (a) $CuInS_2$ and (b) Zn-CIS.

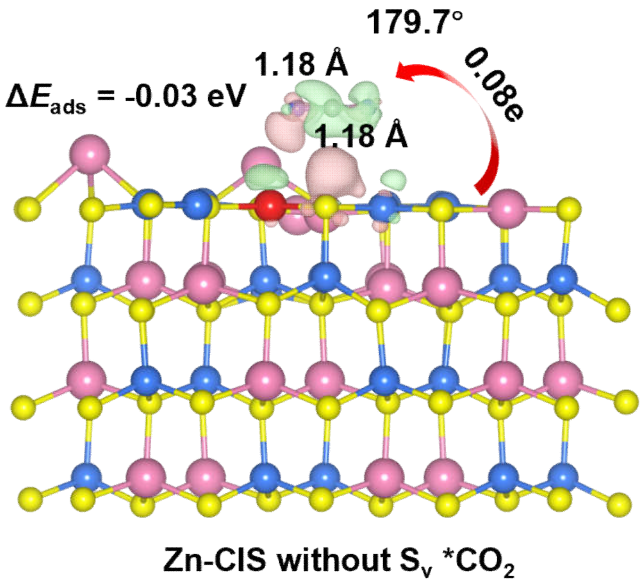

Fig. S15. CO_2 adsorption model, differential charge and bader charge of Zn-CIS without S_v (the electron–density isosurface was plotted at 0.0004 e $Å^{-3}$, the pink and green zones indicate electron accumulation and depletion)

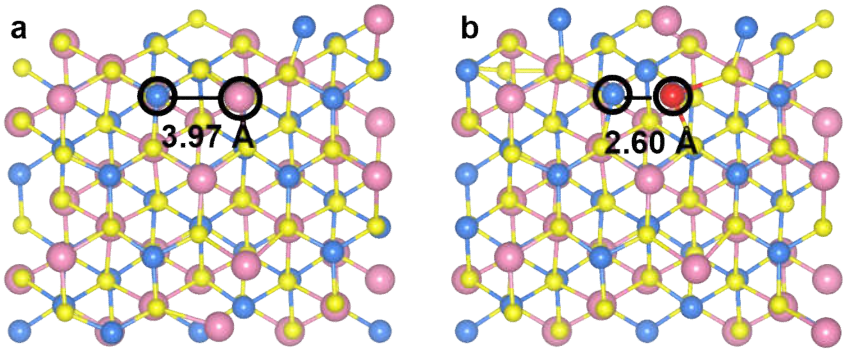

Fig. S16. The top view of $CuInS_2$ model and Zn-CIS model.

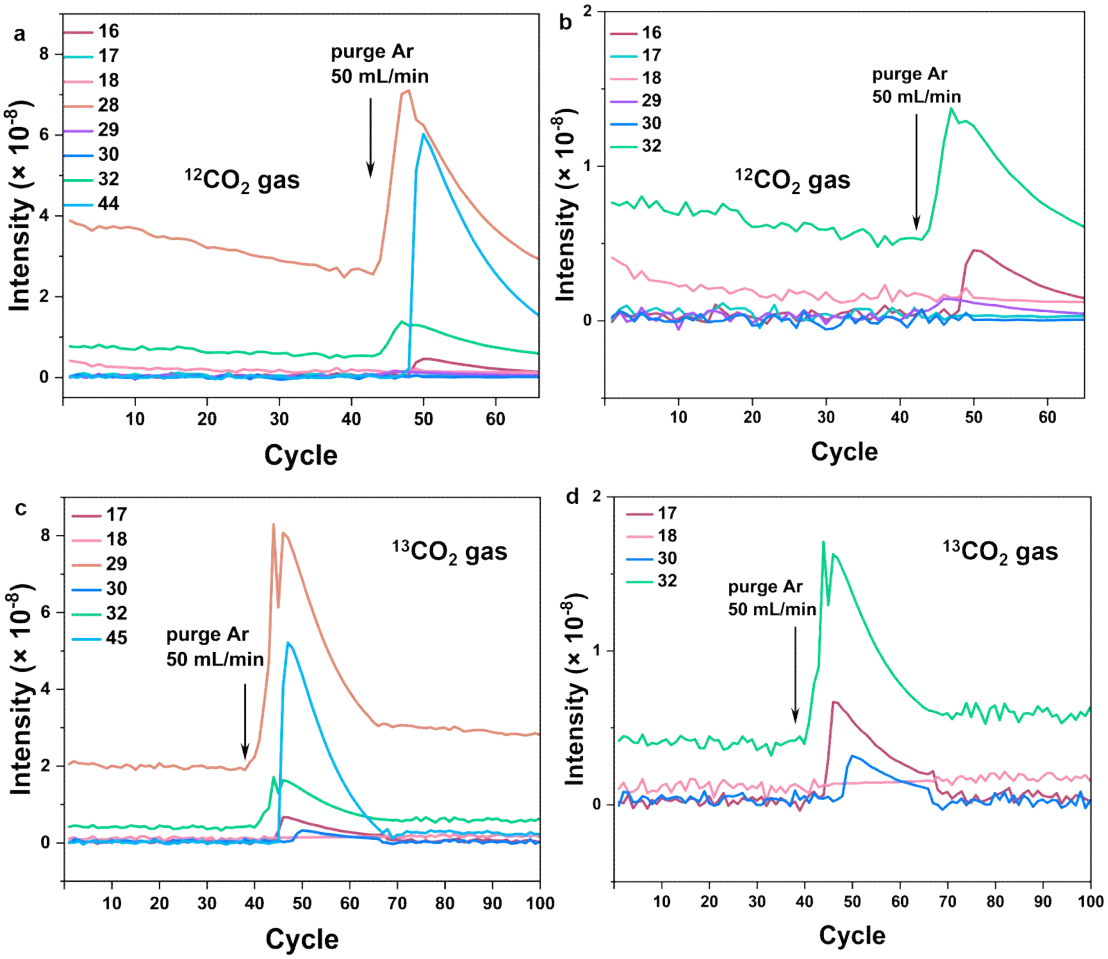

Fig. S17. The mass spectrometry spectrum of $^{12}CO_2$ (a, b) and $^{13}CO_2$ (c, d) isotope experiments on 3Zn-CIS.

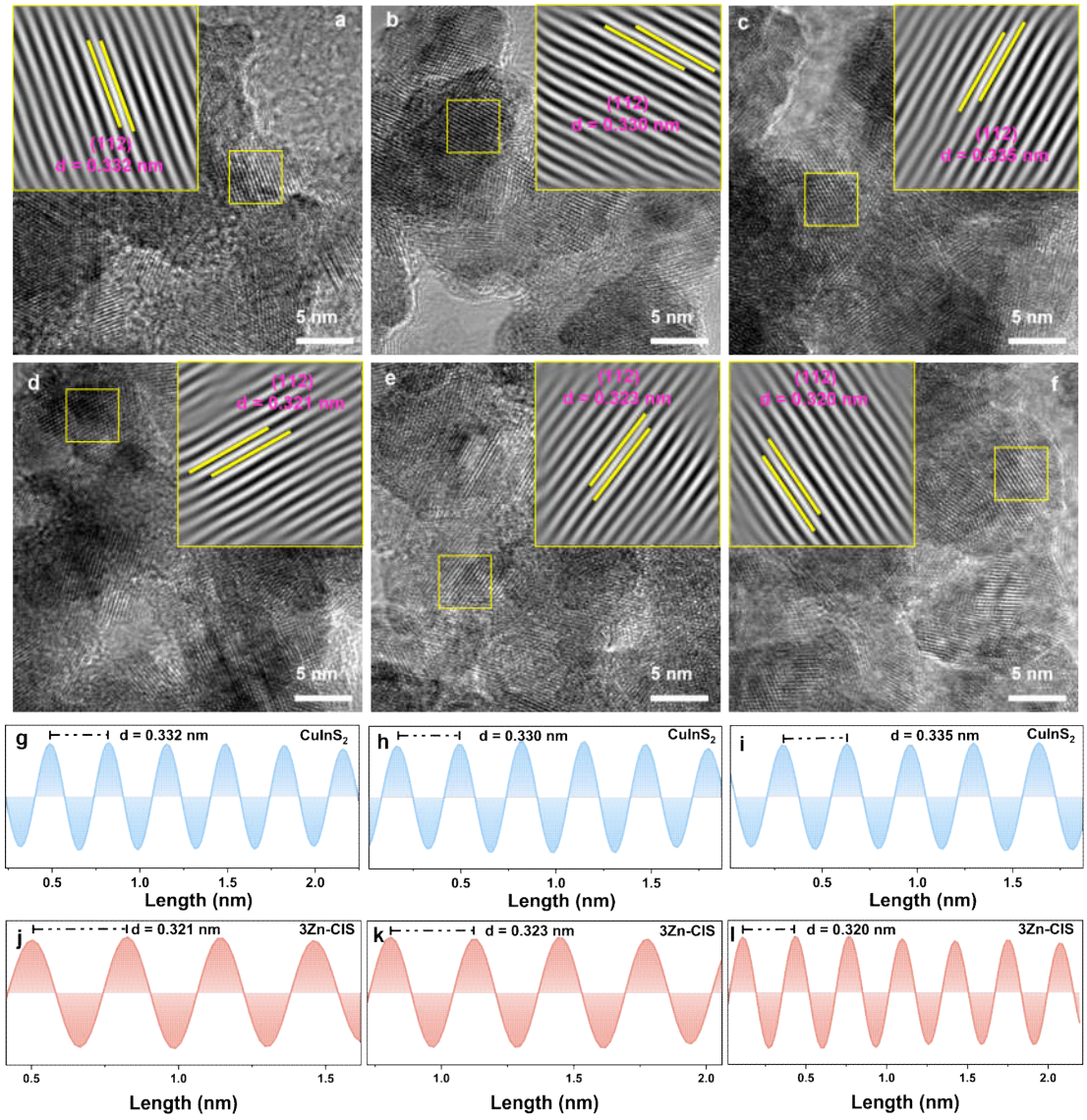

Fig. S18. The HRTEM images and corresponding interplanar spacing of $CuInS_2$ (a, g; b, h; c, i) and 3Zn-CIS (d, j; e, k; f, l).

2. Supplementary Tables

Table S1. Mass percent of Zn element of xZn-CIS from ICP-OES.

Sample	Mass persentage (%)
1Zn-CIS	0.87
3Zn-CIS	1.69
5Zn-CIS	2.07

Table S2. Crystallographic data of the $CuInS_2$ and xZn-CIS by Rietveld refinement.

Sample	***a* (Å)**	***b* (Å)**	***c* (Å)**	***α* (°)**	***β* (°)**	***γ* (°)**	**cell volume (Å^3)**
$CuInS_2$	5.474	5.474	10.629	90	90	90	318.45
1Zn-CIS	5.467	5.467	10.624	90	90	90	317.5
3Zn-CIS	5.460	5.460	10.619	90	90	90	316.6
5Zn-CIS	5.458	5.458	10.611	90	90	90	316.17

Table S3. EXAFS fitting parameters at the Zn K-edge for various samples (S_0^2=0.850)

Sample	shell	CN[a]	R[b](Å)	σ²[c](Å²)	ΔE₀[d](eV)	R factor
Zn foil	Zn–Zn	6*	2.64 ± 0.01	0.0101	1.3 ± 0.6	0.006
ZnS	Zn–S	4*	2.32 ± 0.02	0.0050	2.9 ± 0.4	0.016
3Zn-CIS	Zn–S	3.06 ± 0.2*	2.27 ± 0.08	0.0079	–6.9 ± 0.2	0.001

[a]*CN*: coordination numbers; [b]*R*: bond distance; [c]σ^2: Debye-Waller factors; [d] ΔE_0: the inner potential correction. R factor: goodness of fit. Error bounds that characterize the structural parameters obtained by EXAFS spectroscopy were estimated as CN ± 20%; R ± 1%; σ^2 ± 20%.

Table S4. Comparison of the recently published catalysts for photocatalytic CO_2 to C_2H_4

Catalysts	Reaction conditions	Light sources	C_2H_4 production rate($\mu mol \cdot g^{-1} \cdot h^{-1}$)	C_2H_4 Selectivity (%)	refs
$Cu^{\delta+}$/ CeO_2-TiO_2	10 mg photocatalysts in 30 mL H_2O, 0.1 MPa CO_2 gas	300 W Xe-lamp, 200 $mW \cdot cm^{-2}$ ($320 > \lambda > 850$ nm)	4.51	73.9	[1]
CuACs/PCN	5 mg photocatalyst in 45 mL H_2O and 5 mL TEOA, CO_2 gas, $C_{30}H_{24}Cl_2N_6Ru \cdot 6H_2O$	300 W Xe-lamp	10.17	63.02	[2]
Au-Pd/TiO_2	0.26 MPa CO_2, 0.1 mL H_2O	300 W Xe-lamp, 853 $mW \cdot cm^{-2}$	14.3	22.75	[3]
Sv-CdS@ZIF-8	80 KPa CO_2, 2 mL H_2O 20 mg photocatalysts, 25 ℃	300 W Xe-lamp ($\lambda > 420$ nm)	0.8	12.8	[4]
CuO_X@p-ZnO	0.5 MPa CO_2 and H_2O, 5 mg photocatalysts	350 W Xe-lamp, 100 $mW \cdot cm^{-2}$ ($320 > \lambda > 780$ nm)	22.3	57.49	[5]
Co-doped NiS_2	10 mg photocatalysts, 10% CO_2 90% N_2, 1 atm	300 W Xe-lamp, 100 $mW \cdot cm^{-2}$ (AM 1.5G solar simulator)	2.5	74.3	[6]
Mo-MOF	10 mg photocatalysts, 5 mL H_2O, CO_2 gas	300 W Xe-lamp ($\lambda > 420$ nm)	3.57	67.1	[7]
$CuInP_2S_6$	4-5 mg photocatalysts, 0.4 mL H_2O, CO_2 gas	300 W Xe-lamp (AM 1.5G solar simulator)	20.89	74.6	[8]
MoS_x/Fe_2O_3	2 mg photocatalysts, 1 mL H_2O, CO_2 gas	300 W Xe-lamp, 100 $mW \cdot cm^{-2}$	10.6	86.17	[9]
$Cu_1/W_{18}O_{49}$	5 mg photocatalysts,200 μL H_2O, CO_2 gas	300 W Xe-lamp, 453 $mW \cdot cm^{-2}$	4.9	67.9	[10]
α-Fe_2O_3/GR/Bi_2O_2S	CO_2 gas and 300 μL H_2O, 80 kPa	300 W Xe-lamp, 100 $mW \cdot cm^2$ ($\lambda > 420$ nm)	2.88	36.5	[11]
V_S-$NiCo_2S_4$-NF	5 mg photocatalysts,0.5 mL H_2O, CO_2 gas	300 W Xe-lamp, 150 $mW \cdot cm^{-2}$	35.4	84.6	[12]
MIL-88B-NS40	5 mg photocatalysts,2 mL H_2O, CO_2 gas	300 W Xe-lamp, 200 $mW \cdot cm^{-2}$ ($\lambda > 420$ nm)	17.7	10.6	[13]
BPQD-WO_3	10 mg photocatalysts, 0.4 mL H_2O, CO_2 gas	300 W Xe-lamp	11	49.2	[14]
$Bi_{19}S_{27}Br_3$-V_S	20 mg photocatalysts, 1 mL H_2O, 80 KPa CO_2, 5 ℃	300 W Xe-lamp	4.75	85	[15]
Co_3S_4/NC@ZnS/NC	35 mg photocatalysts, CO_2 gas, 25℃	300 W Xe-lamp, 920 $mW \cdot cm^2$ ($\lambda > 420$ nm)	12.23	66.98	[16]
In_2S_3@Bi_2S_3	5 mg photocatalysts, 1 mL H_2O, CO_2 gas	300 W Xe-lamp	11.81	97.35	[17]
Zn-$CuInS_2$	10 mg photocatalyst, 1.68 g $NaHCO_3$ and 15 mL 0.5 M H_2SO_4, 25 °C	300 W Xe-lamp, 600 $mW \cdot cm^{-2}$ ($\lambda > 420$ nm)	15.9	77.5	This work

3. Reference

[1] T. Wang, L. Chen, C. Chen, M. Huang, Y. Huang, S. Liu, B. Li, *ACS Nano*, **2022**, 16, 2306–2318.

[2] W. Xie, K. Li, X.-H. Liu, X. Zhang, H. Huang, *Adv. Mater.*, **2023**, 35, 2208132.

[3] Q. Chen, X. Chen, M. Fang, J. Chen, Y. Li, Z. Xie, Q. Kuang, L. Zheng, *J. Mater. Chem. A,* **2019**, 7, 1334–1340.

[4] F. Tian, H. Zhang, S. Liu, T. Wu, J. Yu, D. Wang, X. Jin, C. Peng, *Appl. Catal. B Environ. Energy*, **2021**, 285, 119834.

[5] W. Wang, C. Deng, S. Xie, Y. Li, W. Zhang, H. Sheng, C. Chen, J. Zhao, *J. Am. Chem. Soc.,* **2021**, 143, 2984–2993.

[6] W. Shao, X. Li, J. Zhu, X. Zu, L. Liang, J. Hu, Y. Pan, J. Zhu, W. Yan, Y. Sun, Y. Xie, *Nano Res.*, **2022**, 15, 1882–1891.

[7] M. Kou, W. Liu, Y. Wang, J. Huang, Y. Chen, Y. Zhou, Y. Chen, M. Ma, K. Lei, H. Xie, P.K. Wong, L. Ye, *Appl. Catal. B Environ. Energy*, **2021**, 291, 120146.

[8] W. Gao, L. Shi, W. Hou, C. Ding, Q. Liu, R. Long, H. Chi, Y. Zhang, X. Xu, X. Ma, Z. Tang, Y. Yang, X. Wang, Q. Shen, Y. Xiong, J. Wang, Z. Zou, Y. Zhou, *Angew. Chem. Int. Ed.*, **2024**, 63, e202317852.

[9] W. Song, C. Wang, Y. Liu, K.C. Chong, X. Zhang, T. Wang, Y. Zhang, B. Li, J. Tian, X. Zhang, X. Wang, B. Yao, X. Wang, Y. Xiao, Y. Yao, X. Mao, Q. He, Z. Lin, Z. Zou, B. Liu, *J. Am. Chem. Soc.*, **2024**, 146, 29028–29039.

[10] Y. Mao, M. Zhang, G. Zhai, S. Si, D. Liu, K. Song, Y. Liu, Z. Wang, Z. Zheng, P. Wang, Y. Dai, H. Cheng, B. Huang, *Adv. Sci.*, **2024**, 11, 2401933.

[11] Y. Luo, H. Han, G. Zhang, Q. Wang, Y. Jia, *Sep. Purif. Technol.* **2023**, 314, 123607.

[12] X. Luo, L. Qiao, S. Zhang, Q. Li, Y. Liao, S. Rao, H. Liu, Y. Zhao, *Appl. Surf. Sci.* **2022**, 601, 154184.

[13] F. Guo, R.-X. Li, S. Yang, X.-Y. Zhang, H. Yu, J.J. Urban, W.-Y. Sun, *Angew. Chem. Int. Ed.* **2023**, 62, e202216232.

[14] W. Gao, X. Bai, Y. Gao, J. Liu, H. He, Y. Yang, Q. Han, X. Wang, X. Wu, J. Wang, F. Fan, Y. Zhou, C. Li, Z. Zou, *Chem. Commun.* **2020**, 56, 7777-7780.

[15] J. Zhao, H. Chen, B. Wang, M. Ji, D. Su, L. Song, P. Zhang, Y. She, Y.-X. Weng, H. Li, J. Xia, *Appl. Catal. B Environ. Energy* **2025**, 361, 124647.

[16] L. Huang, S. Mo, X. Zhao, J. Zhou, X. Zhou, Y. Zhang, Y. Fan, Q. Xie, B. Li, J. Li, *Appl. Catal. B Environ. Energy* **2024**, 352, 124019.

[17] K. Yan, D. Wu, T. Wang, C. Chen, S. Liu, Y. Hu, C. Gao, H. Chen, B. Li, *ACS Catal.* **2023**, 13, 2302–2312.